Available online at www.sciencedirect.com
ScienceDirect
Trans. Nonferrous Met. Soc. China 20(2010) 2129−2133
Transactions of Nonferrous Metals Society of China
www.tnmsc.cn

Aluminum matrix composites reinforced by in situ Al_2O_3 and Al_3Zr particles fabricated via magnetochemistry reaction

ZHAO Yu-tao(赵玉涛), ZHANG Song-li(张松利), CHEN Gang(陈 刚)

School of Materials Science and Engineering, Jiangsu University, Zhenjiang 212013, China

Received 23 October 2009; accepted 16 September 2010

Abstract: Aluminum matrix composites reinforced by in situ Al_2O_3 and Al_3Zr particles are fabricated from A356-Zr$(CO_3)_2$ system via magnetochemistry reaction, and the morphologies, sizes and distributions of the in situ particles as well as the microstructures, mechanical mechanisms of the composites are investigated by XRD, SEM, TEM and in situ tensile tests. The results indicate that with the pulsed magnetic field assistance, the morphologies of the in situ particles are mainly with ball-shape, the sizes are in nanometer scale and the distributions in the matrix are uniform. The interfaces between the in situ particles and the aluminum matrix are net and no interfacial outgrowth is observed. These are due to the strong vibration induced by the applied magnetic field in the aluminum melt, which in turn, accelerates the melt reactions. The effects of the magnetic field on the above contributions are discussed in detail.

Key words: aluminum matrix composites; magnetochemistry reaction; Al_2O_3; Al_3Zr; in situ tensile

1 Introduction

Particle-reinforcement aluminum metal matrix composites (PRAMMCs) are attractive for the materials scientists to meet the increasing demands of applying advanced structures in aerospace, military, automobile and electronic areas because of their low density, high specific stiffness, strong wear resistance, reduced thermal expansion coefficient and high thermal conductivity, such as aerofoil, motor cylinder body, braking pan[1−5]. PRAMMCs can be fabricated by ex-situ synthesis (e.g. liquid ingot casting and powder metallurgy) where particles are added to the melt as a powder, and also by in-situ synthesis (e.g. exothermic dispersion, reactive hot pressing, reactive infiltration and direct melt reaction) where particles are synthesized within the melt[6−12]. In ex-situ methods, the particles are added into the metal melt from the outside, which induces interface pollution, poor wetting ability and weak properties of the composites. In in-situ process, the reinforcement phases are formed in the matrix metal from chemical reactions or from exothermic reactions between elemental powders of the composite under hot pressing conditions, which are thermodynamically stable, free of surface contamination and disperse more uniformly, leading to stronger particle-matrix bonding. Such unique properties make the in-situ PRAMMCs possess excellent mechanical properties and economical viability than their ex-situ counterparts. In particular, the direct melt reaction (DMR) process is the most promising in-situ synthesis techniques for commercial applications due to its simplicity, low cost and near net-shape forming capability. In the conventional DMR processing, long agitating time at high temperature is necessary for obtaining full incorporation and thorough reaction of the added reactants with the molten metal. These lead to the in situ particles growing up or agglomerating together and more melt being lost, and induce the properties decreasing. In order to shorten the long mixing time at high temperature, some researches have been done[13−15].

In the present work, the aluminum matrix composites reinforced by Al_2O_3 and Al_3Zr particles are fabricated from an A356-Zr$(CO_3)_2$ system through magnetochemistry reaction, and the morphologies, sizes and distributions of the in situ particles as well as the microstructures, mechanical mechanisms of the

Foundation item: Project(2007AA03Z548) supported by High-Tech Research and Development Program of China; Project(50971066) supported by the National Natural Science Foundation of China; Project(1283000349) supported by the Jiangsu University Research Fund for Advanced Scholars, China

Corresponding author: ZHAO Yu-tao; Tel: +86-511-88797658; E-mail: zsl@ujs.edu.cn; zhaoyt@ujs.edu.cn

DOI: 10.1016/S1003-6326(09)60429-5

composites are investigated by XRD, SEM, TEM and in-situ tensile observations. The effects of the magnetic field on the above contributions are discussed in detail.

2 Experimental

The starting materials were commercial A356 alloy ingots and inorganic salt $Zr(CO_3)_2$ powder.

Firstly, $Zr(CO_3)_2$ powders were dehydrated at 250 °C for 3 h in an electric furnace. Then aluminum ingots were heated to 900 °C and melted, the dried $Zr(CO_3)_2$ powders with the mass fraction of 20% to the total aluminum melt were added and pressed into the aluminum melt with a campanulate graphite mantle. During the in situ reaction, the impulse magnetic field system (WY1600) was turned on and the frequency was fixed at 25 Hz and the magnetic current intensity was 150 A. The parameters of pulsed magnetic field were voltage 550 V, current 10 A, frequency 100 kHz and pulse width 10 ms. After 20 min, the melt was degassed by hexachloroethane degasifying agent, deslagged, and then poured into a mould with 14 mm inner diameter. After being cooled to room temperature in air, the specimens for XRD, SEM and TEM analyses, mechanical properties testing and in situ tension test were processed. The tensile properties are the average values of three tests.

SEM(JOEL-JXA-840) with a microtensile holder was used to investigate the microstructure of the as-prepared specimens and the in-situ tensile test, and TEM(JSM2010) for the morphologies and the interfaces. Tensile properties tests of the specimens with a gauge diameter of 6.35 mm and length of 25.4 mm were carried out at room temperature by a computer-controlled electronic tensile testing machine (DWD-200) at a strain rate of $1.67\times10^{-4}\ s^{-1}$ according to the ASTM E8 standard. The Brinell Hardness was determined by THI100 electronic-controller type hardness testing device according to the ASTM E10 standard. The values of the tensile properties and Brinell hardness are the average of three tests at each condition, respectively.

3 Results and discussion

3.1 XRD pattern

Fig.1 shows the XRD pattern of the composites fabricated with pulsed magnetic field assistance. It indicates that Al, Al_2O_3 and Al_3Zr phases are obtained. These mean that some chemical reactions occur in the aluminum melt: the $Zr(CO_3)_2$ are decomposed to ZrO_2 particles and CO_2 gas. The decomposed products ZrO_2 react with aluminum, and CO_2 gas is partly escaped out of the aluminum melt and the residual is degassed by degasifying agent. Zirconium atom in ZrO_2 is substituted by aluminum atom and Al_2O_3 particles are formed. The substituted zirconium atom in aluminum melt also reacts with aluminum atom, and Al_3Zr particles are formed. The total melt chemical reactions can be expressed as:

$$3Zr(CO_3)_2+13Al(l)\longrightarrow 6CO_2\uparrow+3Al_3Zr+2Al_2O_3 \quad (1)$$

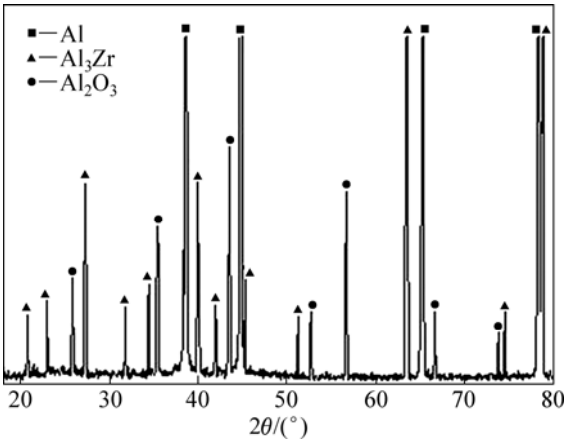

Fig.1 XRD pattern of composites fabricated with pulsed magnetic field assistance

3.2 SEM images

Fig.2 shows the SEM images of the composites prepared without and with pulsed magnetic field assistance. It can be clearly seen that with the assistance of pulsed magnetic field, the distributions of the in-situ Al_2O_3 and Al_3Zr particles become more uniform, the size

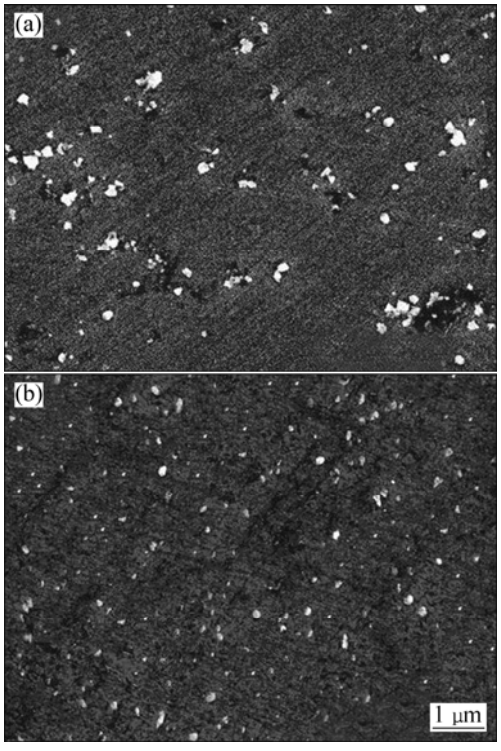

Fig.2 SEM images of in-situ particles reinforced composites fabricated without pulsed magnetic field assistance (a) and with pulsed magnetic field assistance (b)

gets more smaller, and the amount of the in-situ particles is increased. The size of particles is in the range of 0.08−0.13 μm, which is much finer than that formed without pulsed magnetic field assistance. These are due to the effects of pulsed magnetic field on the in-situ melt chemical reactions.

3.3 TEM micrographs

Fig.3 shows the TEM micrograph of the Al_3Zr/Al and α-Al_2O_3/Al interfaces and the electron diffraction patterns, respectively. The diffraction patterns of the A, B, C and D regions are determined as Al_3Zr phase, Al phase, α-Al_2O_3 phase and Al phase according to the standard diffraction patterns. Thus, the interfaces between A and B, C and D regions are the Al_3Zr/Al and α-Al_2O_3/Al interfaces, separately. As shown in Figs.3(a) and (b), the interfaces are smooth, round and net. These contribute to the interface bond strength.

3.4 Effects of magnetic field on microstructure of composite

In aluminum melt, when the pulsed magnetic field is applied, the alternating current generates the pulsed magnetic field B in the melt, which in turn, induces the pulsed eddy current J_e in melt according to laws of Faraday electromagnetism induction. Therefore, the aluminum melt is subjected to electromagnetic body forces $\boldsymbol{f}$ caused by the interaction of the induced current J_e and the magnetic filed B. Based on Maxwell's equations, $\nabla \times \boldsymbol{B} = \mu_0 J_e$, the electromagnetic forces $\boldsymbol{f}$, which is a dependent variable to the volume of the aluminum melt, can be described by the following equation:

$$\boldsymbol{f} = \frac{1}{\mu_0}\left[(\boldsymbol{B}\cdot\nabla)\boldsymbol{B} - \frac{1}{2}\nabla \boldsymbol{B}^2\right] \tag{2}$$

where μ_0 is the permeability of the aluminum melt, and $\boldsymbol{B}$ the magnetic filed intensity. According to Maxwell equation, Eq.(2) integrated to the volume can be written as:

$$\int \boldsymbol{f}\mathrm{d}v = \frac{1}{\mu_0}\left[\int \boldsymbol{B}^2 \boldsymbol{b}\cos\theta - \frac{\boldsymbol{B}^2}{2}\boldsymbol{n}\right]\mathrm{d}s \tag{3}$$

where $\boldsymbol{b}$ is the unit vector in the direction of the impulse magnetic field, $\boldsymbol{n}$ the outer-normal unit vector of the integral unit, θ the separation angle between $\boldsymbol{b}$ and $\boldsymbol{n}$. The magnetic intensity in the inner of the aluminum melt is generated by the two parts indicated in the right of Eq.(3). The pulsed magnetic field B changes at a high rate. These generate strong vibration in the aluminum melt, which in turn, induces violence convection current. These contribute to the uniform distribution of the reinforcements in the aluminum matrix.

In the Al-$Zr(CO_3)_2$ system, the following chemical reaction is important to the formation of Al_2O_3 and Al_3Zr phases:

$$4Al(l)+3ZrO_2 \longrightarrow 2Al_2O_3+3[Zr] \tag{4}$$

Reaction (4) can be expressed as:

$$4Al+3ZrO_2 \longrightarrow [3Zr\cdot 6O\cdot 4Al] \longrightarrow 2Al_2O_3+3Zr \tag{5}$$

The reaction (5) indicates that ZrO_2 particles are wetted with aluminum molten, and then transformed into intermediate products. After complex chemical transition, the simple substance Zr and Al_2O_3 particles are produced, and promptly diffused out of the reaction transition regions. The Zr reacts with aluminum to form Al_3Zr particles.

When pulsed magnetic field is applied, the practical reaction rate coefficient K can be written as $K=K_t+K_m$, where K_m comes from the magnetic field contributions. The reaction rate, which is represented by the volume mole concentration of Al_2O_3 particles can be expressed as:

$$\frac{\mathrm{d}C_{Al_2O_3}}{\mathrm{d}t} = K' C_{Al}^4 C_{ZrO_2}^3 = (K_t + K_m) C_{Al}^4 C_{ZrO_2}^3 \tag{6}$$

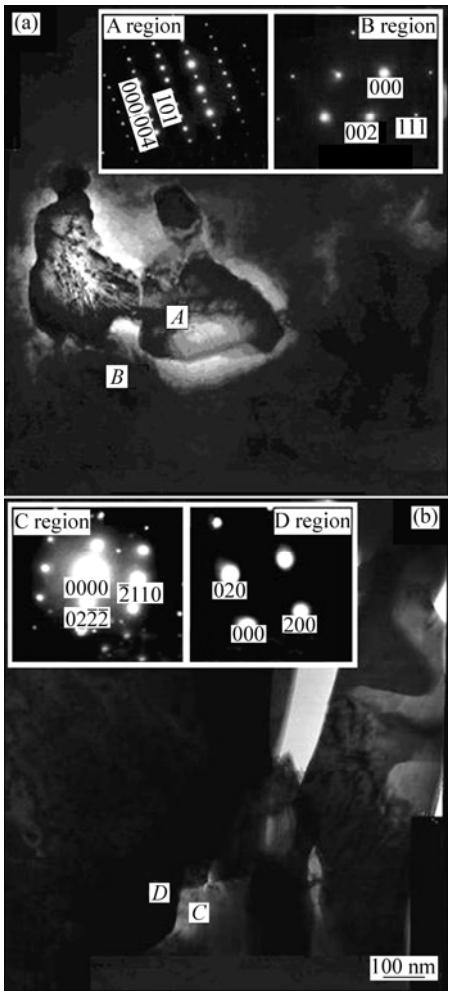

Fig.3 TEM micrographs of Al_3Zr/Al and α-Al_2O_3/Al interfaces and electron diffraction patterns

Thus, the reaction coefficient is magnified due to the K_m and the chemical reaction is accelerated.

3.5 Mechanical properties

The mechanical properties of the as-prepared composites fabricated with and without the assistance of pulsed magnetic field are listed in Table 1. It indicates that the values of the tensile strength, yield strength and the hardness are increased with the pulsed magnetic field assistance, reaching 393.87 MPa, 339.74 MPa and 139.8 N/mm^2, respectively, and the values of the elongation show no obvious variations.

Table 1 Mechanical properties of composites fabricated with and without pulsed magnetic field assistance

Pulsed magnetic field assistance	Tensile strength/ MPa	Yield strength/ MPa	Elongation/%	Brinell hardness/ (N·mm^{-2})
Without	345.76	278.95	4.85	108.4
With	393.87	339.74	4.72	139.8

Fig.4 shows the SEM micrographs of the crack initiating course and the crack growing course for the as-prepared composites. In the initiating stage shown in Figs.4(a)−(c), the white-fine interleaving slipping bands with obvious convex-concave marks are clearly seen. The observed short-tenuous breaches are grown and joined together, which induces to the micro-cracks birth and growth. When the master cracks expand and meet with the rich-particle areas, the extending direction turns to the poor-particle areas, the bottleneck of the cracks is generated, and the crack expanding is continued along the boundary between the particle-rich and the particle-poor areas. With the load increasing, the rich-particle areas are desquamated from the aluminum matrix and the composites are breakdown. Thus, the tensile strength is inactivation.

Fig.5 shows the SEM images of the tensile fracture surface of the as-prepared composites synthesized without and with pulsed magnetic field assistance, respectively. The obvious dimple-shape appearances of the fracture surfaces are seen in the fracture surface. With the pulsed magnetic field assistance, the amounts of

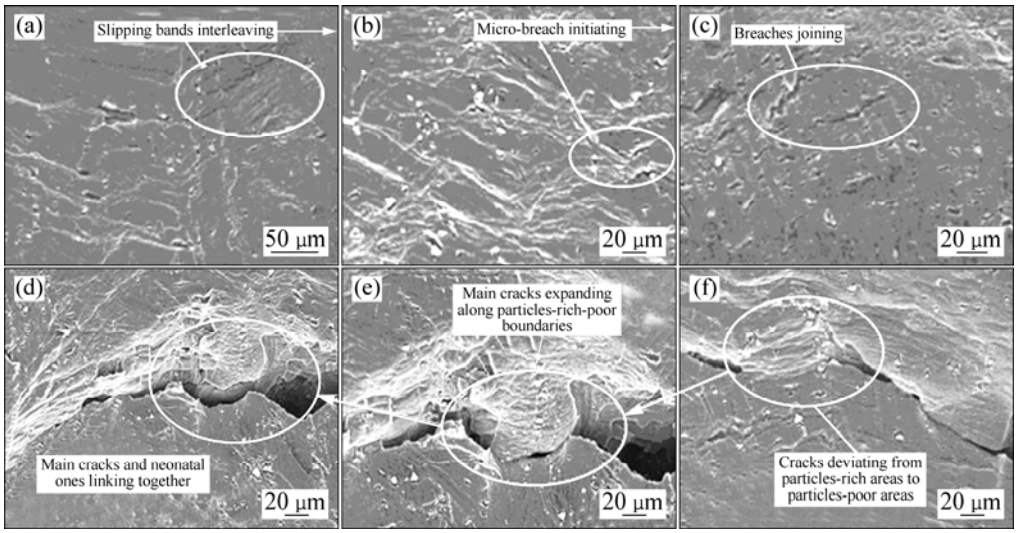

Fig.4 SEM micrographs of crack initiating and growing course for (Al_3Zr+Al_2O_3)/A356 composites

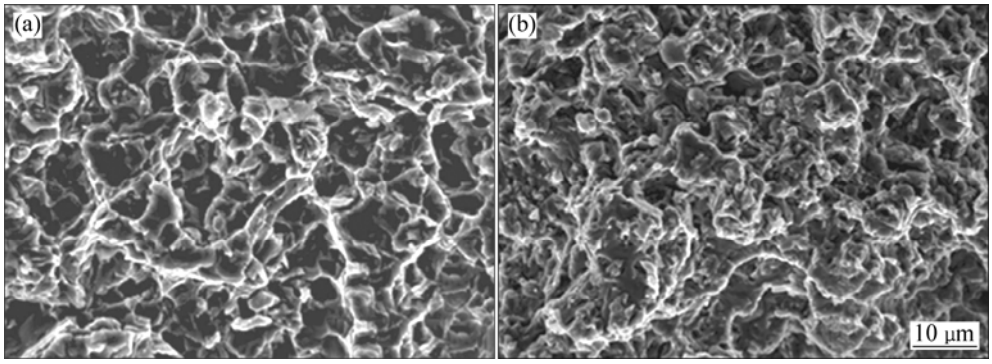

Fig.5 SEM images of tensile fracture surface of as-prepared composites synthesized without (a) and with (b) pulsed magnetic field assistance

the observed dimples increases, and the sizes reduce, comparing to that without pulsed magnetic field assistance. These contribute to the mechanical properties of the composites.

4 Conclusions

The aluminum matrix composites reinforced by in situ Al_2O_3 and Al_3Zr particles are fabricated from A356-$Zr(CO_3)_2$ system via magnetochemistry reaction, and the morphologies, sizes and distributions of the in situ particles as well as the microstructures, mechanical mechanisms of the composites are investigated. The results indicate that with the pulsed magnetic field assistance, the morphologies of the in situ particles are ball-shape, the sizes are in nanometer scale and the distributions are uniform in the matrix. The interfaces between the in situ particles and the aluminum matrix are net and no interfacial outgrowth is observed. The values of the tensile strength, yield strength and the Brinell hardness reach 393.8 MPa, 339.74 MPa and 139.8 N/mm^2, respectively. The in situ tensile observations show that the cracks are initiated by the dislocation accumulation effects, the cavity-nucleation effects and the matrix fracture effects; the crack growth behaviors are very much dependent on the microstructure of the composites. These are due to the strong vibration induced by the applied magnetic field in the aluminum melt, which in turn, accelerates the melt reactions.

References

[1] QI Qing-ju. Evaluation of sliding wear behavior of graphite particle-containing magnesium alloy composites [J]. Transactions of Nonferrous Metals Society of China, 2006, 16(5): 1135−1140.

[2] KANG Y C, CHAN S L I. Tensile properties of nanometric Al_2O_3 particulate-reinforced aluminum matrix composites [J]. Materials Chemistry and Physics, 2004, 85(2/3): 438−443.

[3] MIYAJIMA T, IWAI Y. Effects of reinforcements on sliding wear behavior of aluminum matrix composites [J]. Wear, 2003, 255(1/6): 606−616.

[4] YUAN W H, CHEN Z H, XU H Y, ZHANG F Q, FU D F. Properties and microstructures of 7075/SiC_p composites prepared by spray deposition [J]. Transactions of Nonferrous Metals Society of China, 2003, 13(5): 1160−1163.

[5] GENG Lin, ZHANG Xue-nan, WANG Gui-song, ZHENG Zhen-zhu, XU Bin. Effect of aging treatment on mechanical properties of (SiCw+SiC_p)/2024Al hybrid nanocomposites [J]. Transactions of Nonferrous Metals Society of China, 2006, 16(2): 387−391.

[6] WOOD J V, DAVIS P, KELLIE J L F. Properties of reactively cast aluminium-TiB_2 alloys [J]. Mater Sci Tech, 1993, 9(9/10): 833−840.

[7] FENG C F, FROYEN L. Formation of Al_3Ti and Al_2O_3 from an Al-TiO_2 system for preparing in-situ aluminium matrix composites [J]. Mater Sci Tech, 2000, 31(4): 385−390.

[8] SHIN K, CHUNG D, LEE S. The effect of consolidation temperature on microstructure and mechanical properties in powder metallurgy-processed 2××× aluminum alloy composites reinforced with SiC particulates [J]. Metall Mater Trans A, 1997, 28(12): 2625−2636.

[9] HONG S H, CHUNG K H. Effects of vacuum hot pressing parameters on the tensile properties and microstructures of SiC-2124Al composites [J]. Materials Science and Engineering A, 1995, 194(2): 165−170.

[10] MITRA R, CHIOU W A, FINE M A, WEERTMAN J R. Interfaces in as-extruded XD Al/TiC and Al/TiB_2 metal matrix composites [J]. Materials Research, 1993, 8(9): 2380−2492.

[11] NAKATA H, CHOH T, KANETAKE N. Fabrication and mechanical properties of in situ formed carbide particulate reinforced aluminium composite [J]. Journal of Materials Science, 1995, 30(7): 1719−1727.

[12] ZHANG Yi-jie, JIANG Sheng-ling, MA Nai-heng, LI Xian-feng, WANG Hao-Wei. Microstructure and properties of in-situ TiB_2 particulates reinforced A356 composite [J]. Transactions of Nonferrous Metals Society of China, 2005, 15(3): 124−127.

[13] ZUO Yu-bo, CUI Jian-zhong, DONG Jie, YU Fu-xiao. Effect of low frequency electromagnetic field on the constituents of a new super high strength aluminum alloy [J]. J Alloys Comps, 2005, 402(1/2): 176−181.

[14] AGUAS M D, AFFLECK L, PARKIN I P, KUZNETSOV M V, et al. The effect of large magnetic fields on solid state combustion reactions: novel microstructure, lattice contraction and reduced coercivity in barium hexaferrite [J]. J Mater Chem, 2000, 10(2): 235−237.

[15] YAMAGUCHI M, YAMAMOTO I, ISHIKAWA F, GOTO T, MIURA S. Thermodynamic theory of magnetic field effects on chemical equilibria and applications to metal-hydrogen systems [J]. J Alloys Comps, 1997, 253/254: 308−312.

(Edited by LAI Hai-hui)